Dufour and Soret Effects on Unsteady MHD Free Convective Flow of Viscous Incompressible Fluid Past an Infinite Vertical Porous Plate in the Presence of Radiation

B. Prabhakar Reddy[1,2*], Jefta M. Sunzu[1]

[1]Department of Mathematics, School of Mathematical Sciences, CNMS, The University of Dodoma, P. Box. No. 338, Dodoma, Tanzania
e-mail: prabhakar.bijjula@gmail.com
[2]Department of Mathematics, Geethanjali College of Engineering & Technology,
Cheeryal (V), Keesara (M), Medchal (Dist) -501301, Telangana, India
e-mail: jefta@aims.ac.za
corresponding author

Abstract

In this paper, the Dufour and Soret effects on an unsteady MHD free convection flow of an incompressible, electrically conducting viscous Newtonian fluid past an infinite vertical porous plate have been studied, taking into account Viscous and Darcy resistance terms and constant permeability of the medium in the presence of radiation. The fluid is considered as a gray, absorbing-emitting but non-scattering medium. The Rosseland approximation in the energy equation is used to describe the radiative heat flux for optically thick fluid. The dimensionless governing equations for this investigation are solved numerically using Galerkin finite element method. The influence of the physical parameters involved in the problem under investigation on the velocity, temperature and concentration profiles within the boundary layer are presented through the graphs and tabulated results for the skin-friction coefficient, Nusselt and Sherwood numbers.

Keywords: MHD, Dufour number, Soret number, radiation parameter, vertical plate

1. Introduction

The problem of free convection heat and mass transfer flows through a porous medium under the influence of magnetic field have been attracting the attention of a number of researchers because of their possible applications in many branches of science and technology, such as in transportation of cooling of re-entry vehicles and rocket boosters, cross-hatching on ablative surfaces and film vaporization in combustion chambers. On the other hand, if the entire system involving the polymer extraction process is placed in a thermally controlled environment, then the thermal radiation effect is significant. Radiative free convective non-Newtonian fluid flows past a wedge embedded in a porous media were reported by Chamkha et al. (2004). Muthucumaraswamy and Janakiraman (2006) dealt with the MHD and radiation effects on moving isothermal vertical plate with variable mass diffusion. Shanker and Gnaneshwar (2007) analysed the radiation effects on MHD flow past an impulsively started infinite vertical plate

through a porous medium with variable temperature and mass diffusion. Ahmed and Sarmah (2009) presented thermal radiation effects on a transient MHD flow with mass transfer past an impulsively fixed infinite vertical plate. Thermal radiation effects on unsteady MHD free convection flow past a vertical plate with temperature dependent viscosity was investigated by Mahmoud (2009). Mukhopadhyay (2009) investigated the effects of thermal radiation on unsteady mixed convection flow and heat transfer over a porous stretching surface in porous medium. Rao and Reddy (2010) studied heat and mass transfer of an unsteady MHD natural convection flow of a rotating fluid past a vertical porous plate in the presence of radiative heat transfer. Shanker et al. (2010) analysed the effects of radiation and mass transfer on an unsteady MHD free convective fluid flow embedded in a porous medium with heat generation/absorption. Muthucumaraswamy and Sivakaumar (2016) studied the MHD flow past a parabolic flow past an infinite isothermal vertical plate in the presence of thermal radiation and chemical reaction.

Due to the importance of the Dufour (diffusion-thermo) and Soret (thermal-diffusion) effects on the fluids with very light molecular weight, as well as medium molecular weight, many investigators studied and reported results on these flows of whom are Eckert and Drake (1972), Dursunkaya and Worek (1992), Anghel et al. (2000) and Postelnicu (2004) are worth mentioning. Alam and Rahman (2005) presented the Dufour and Soret effects on MHD free convective heat and mass transfer flow past a vertical flat plate embedded in a porous medium. Alam et al. (2006) investigated the Dufour and Soret effects on unsteady MHD free convection and mass transfer flow past a vertical porous plate in a porous medium. Dufour and Soret effects on steady MHD combined free-forced convective and mass transfer flow past a semi-infinite vertical plate were analyzed by Alam et al. (2006). Mansour et al. (2006) investigated the effects of chemical reaction and thermal stratification on MHD free convective heat and mass transfer over a vertical stretching surface embedded in a porous media by considering Soret and Dufour effects. Vempati and Laxmi Narayana (2010) analysed the Soret and Dufour effects on unsteady MHD flow past an infinite vertical porous plate with thermal radiation and oscillatory suction velocity. Bhagwat et al. (2010) presented the effects of thermal diffusion on MHD free convective flow past a vertical porous plate by taking into account viscous and Darcy resistance terms. MHD natural convection flow past an impulsively moving vertical plate with ramped wall temperature in the presence of thermal diffusion and heat absorption were reported by Seth et al. (2010). The effects of thermal diffusion and viscous dissipation on unsteady MHD free convection flow past a vertical porous plate under oscillatory suction velocity was investigated by Reddy (2014). Venkateswarlu et al. (2014) analysed the thermal diffusion and radiation effects on unsteady MHD free convection heat and mass transfer flow past a linearly accelerated vertical porous plate with variable temperature and mass diffusion.

The purpose of this paper is to analyse the unsteady hydro-magnetic free convection flow past a vertical porous plate taking into account Viscous and Darcy resistance terms and constant permeability of the medium. The aim of the present study is to extend the results of Bhagwat et al. (2010) by incorporating the effects of Dufour and radiation, due to numerous industrial and engineering applications. The Galerkin FEM has been adopted to solve the dimensionless governing of the flow, which is more economical from computational point of view. The effects of the physical parameters on the velocity, temperature and concentration profiles as well as the skin-friction coefficient, Nusselt and Sherwood numbers are presented through the graphs and tables and then discussed.

2. Mathematical Model

An unsteady two-dimensional flow of an incompressible, electrically conducting, viscous Newtonian fluid past an infinite vertical porous plate, taking into account Viscous and Darcy's

resistance terms and constant permeability of the medium in the presence of radiation, is considered. The fluid is considered as a gray absorbing-emitting but non-scattering medium. In the coordinate system, the $x'-$ axis is taken along the plate in the upward direction and $y'-$ axis is taken normal to the plate. A magnetic field of strength B_0 is applied transversely to the direction of the flow. The magnetic Reynolds number is assumed to be very small so that induced magnetic field is neglected. The suction velocity normal to the plate is assumed to be a function of time i.e., $v' = -U_0$, where the minus sign indicates the suction directed towards the plate. Initially ($t' = 0$), the plate and fluid are at the same temperature T_∞' and concentration C_∞' at all points. Subsequently, $t' > 0$, the plate temperature rises to T_w' and the concentration level at the plate rises to C_w'. The flow configuration and the coordinate system are shown in Fig. 1.
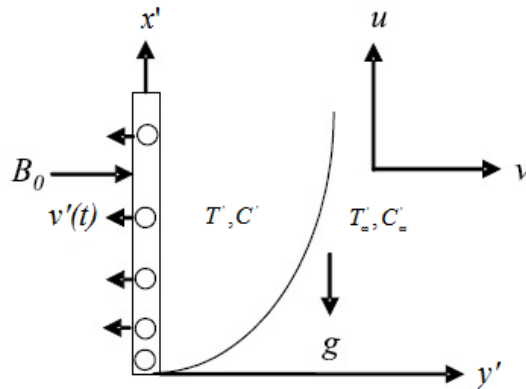

Fig. 1. Flow configuration and coordinate system

The fluid is assumed to have constant properties except that the influence of the density varies with temperature and concentration, which are considered only in the body force term. Under the above assumptions, the physical variables are the functions on y' and t' only. Assuming Boussinesq approximation and boundary layer approximation hold, the basic equations which govern the problem are given by:

$$\frac{\partial v'}{\partial y'} = 0 \tag{1}$$

$$\frac{\partial u'}{\partial t'} + v' \frac{\partial u'}{\partial y'} = g\beta(T'-T_\infty') + g\beta^*(C'-C_\infty') + \upsilon \frac{\partial^2 u'}{\partial y'^2} - \frac{\upsilon u'}{K'} - \frac{\sigma B_0^2 u'}{\rho} \tag{2}$$

$$\frac{\partial T'}{\partial t'} + v' \frac{\partial T'}{\partial y'} = \frac{k}{\rho c_p} \frac{\partial^2 T'}{\partial y'^2} - \frac{\partial q_r^*}{\partial y'} + \frac{D_m k_T}{C_s c_p} \frac{\partial^2 C'}{\partial y'^2} \tag{3}$$

$$\frac{\partial C'}{\partial t'} + v' \frac{\partial C'}{\partial y'} = D_M \frac{\partial^2 C'}{\partial y'^2} + \frac{D_m k_T}{T_m} \frac{\partial^2 T'}{\partial y'^2} \tag{4}$$

with the initial and boundary conditions for the velocity, temperature and concentration fields:

$$t' \le 0; \rightarrow u' = 0, T' = T'_\infty, C' = C'_\infty \dots\dots \text{for all } y'$$

$$t' > 0; \rightarrow u' = 0, T' = T'_w, C' = C'_w \dots\dots \text{at } y' = 0$$

$$u' = 0, T' = T'_\infty, C' = C'_\infty \dots\dots \text{as } y' \rightarrow \infty \qquad (5)$$

where u' and v' are the velocity components in the x' and $y'-$ directions respectively, g is the acceleration due to gravity, β is the volumetric coefficient of thermal expansion, β^* is the volumetric coefficient of concentration expansion, t' is the time, T' is the temperature of the fluid, T'_∞ is the temperature of the fluid far away from the plate, T'_w is the temperature at the plate, C' is the species concentration in the fluid, C'_∞ is the concentration in the fluid far away from the plate, C'_w is the species concentration at the plate, k is the thermal conductivity, υ is the kinematic viscosity, ρ is the fluid density, σ is the electrical conductivity, c_p is the specific heat at constant pressure, q_r^* is the radiative heat flux, D_M is the mass diffusivity, T_m is the mean fluid temperature, C_s is the concentration susceptibility, k_T is the thermal diffusion ratio. The radiative heat flux q_r^* under the Rosseland approximation has the form:

$$q_r^* = -\frac{4\sigma^*}{3k^*} \frac{\partial T'^4}{\partial y'} \qquad (6)$$

where σ^* is the Stefan-Boltzmann constant and k^* is the mean absorption coefficient. It is assumed that the temperature differences within the flow are sufficiently small such that the term T'^4 is expressed as the linear function of temperature. Thus expanding T'^4 about T'_∞ using the Taylor series and neglecting higher order terms, one obtains:

$$T'^4 \simeq T'^4_\infty + 4T'^3_\infty (T' - T'_\infty) \simeq 4T'^3_\infty T' - 3T'^4_\infty$$

Eq. (6) gives

$$q_r^* = -\frac{16\sigma^* T'^3_\infty}{3k^*} \frac{\partial T'}{\partial y'} \qquad (7)$$

From Eqs. (7) and (2) we arrive at the modified energy equation:

$$\frac{\partial T'}{\partial t'} + v' \frac{\partial T'}{\partial y'} = \frac{k}{\rho c_p} \frac{\partial^2 T'}{\partial y'^2} + \frac{16\sigma^* T'^3_\infty}{3k^*} \frac{\partial^2 T'}{\partial y'^2} + \frac{D_m k_T}{C_s c_p} \frac{\partial^2 C'}{\partial y'^2} \qquad (8)$$

Let us introduce the following non-dimensional quantities:

$$u = \frac{u'}{U_0'}, y = \frac{y'U_0'}{v}, t = \frac{t'U_0'^2}{v}, P_r = \frac{\mu c_p}{k}, S_c = \frac{v}{D_M}, M = \frac{\sigma B_0^2 v}{\rho U_0'^2}, K = \frac{U_0^2 K'}{v^2}, H = M + \frac{1}{K},$$

$$N = \frac{\beta^*(C_w' - C_\infty')}{\beta(T_w' - T_\infty')}, \theta = \frac{(T' - T_\infty')}{(T_w' - T_\infty')}, \phi = \frac{(C' - C_\infty')}{(C_w' - C_\infty')}, R = \frac{16\sigma^* T_\infty'^3}{3k^*}, F^* = \frac{P_r}{1+R}, \quad (9)$$

$$D_u = \frac{D_m k_T (C_w' - C_\infty')}{C_s c_p v(T_w' - T_\infty')}, S_r = \frac{D_M k_T (T_w' - T_\infty')}{T_m v(C_w' - C_\infty')}, G_r = \frac{g\beta v(T_w' - T_\infty')}{U_0^3}.$$

where $P_r, S_c, M, K, N, D_u, R, S_r$ and G_r are the Prandtl number, Schmidt number, magnetic parameter, permeability parameter, buoyancy ratio, Dufour number, radiation parameter, Soret number and Grashof number and the other symbols have their usual meaning. The last term on the right hand side of the concentration Eq. (4) and energy Eq. (8) signifies the Soret or thermal-diffusion effect and Dufour or diffusion-thermo effect, respectively.

Using Eq. (9) into Eqs. (2), (4), (5) and (8) we obtain the following governing equations in dimensionless form:

$$\frac{\partial u}{\partial t} - \frac{\partial u}{\partial y} = G_r(\theta + N\phi) + \frac{\partial^2 u}{\partial y^2} - Hu \quad (10)$$

$$\frac{\partial \theta}{\partial t} - \frac{\partial \theta}{\partial y} = \frac{1}{F^*}\frac{\partial^2 \theta}{\partial y^2} + D_u\left(\frac{\partial^2 \phi}{\partial y^2}\right) \quad (11)$$

$$\frac{\partial \phi}{\partial t} - \frac{\partial \phi}{\partial y} = \frac{1}{S_c}\frac{\partial^2 \phi}{\partial y^2} + S_r\left(\frac{\partial^2 \theta}{\partial y^2}\right) \quad (12)$$

with dimensionless initial and boundary conditions:

$$t \leq 0; u = 0, \theta = 0, \phi = 0 \dots\dots \text{for all } y$$
$$t > 0; u = 0, \theta = 1, \phi = 1 \dots\dots \text{at } y = 0$$
$$u = 0, \theta = 0, \phi = 0 \dots\dots \text{ as } y \to \infty \quad (13)$$

3. Method of solution

The Galerkin expression for Eq. (10) over the two-nodded linear element $(e), (y_j \leq y \leq y_k)$ is given by:

$$\int_{y_j}^{y_k} \psi^{(e)T}\left(\frac{\partial^2 u^{(e)}}{\partial y^2} + \frac{\partial u^{(e)}}{\partial y} - Hu^{(e)} - \frac{\partial u^{(e)}}{\partial t} + \Delta\right)dy = 0 \quad (14)$$

where $\psi^{(e)T} = \begin{bmatrix} \psi_j & \psi_k \end{bmatrix}^T = \begin{bmatrix} \psi_j \\ \psi_k \end{bmatrix}$ and $\Delta = G_r(\theta + N\phi)$.

Let $u^{(e)} = \psi_j(y)u_j(t) + \psi_k(y)u_k(t) = \psi_j u_j + \psi_k u_k$ be the linear approximation solution over the element $(e), (y_j \leq y \leq y_k)$. From Eq. (14) the element equation is given by:

$$\int_{y_j}^{y_k} \begin{bmatrix} \psi'_j\psi'_j & \psi'_j\psi'_k \\ \psi'_k\psi'_j & \psi'_k\psi'_k \end{bmatrix}\begin{bmatrix} u_j \\ u_k \end{bmatrix}dy - \int_{y_j}^{y_k} \begin{bmatrix} \psi_j\psi'_j & \psi_j\psi'_k \\ \psi_k\psi'_j & \psi_k\psi'_k \end{bmatrix}\begin{bmatrix} u_j \\ u_k \end{bmatrix}dy +$$

$$H\int_{y_j}^{y_k} \begin{bmatrix} \psi_j\psi_j & \psi_j\psi_k \\ \psi_k\psi_j & \psi_k\psi_k \end{bmatrix}\begin{bmatrix} u_j \\ u_k \end{bmatrix}dy + \int_{y_j}^{y_k} \begin{bmatrix} \psi_j\psi_j & \psi_j\psi_k \\ \psi_k\psi_j & \psi_k\psi_k \end{bmatrix}\begin{bmatrix} u_j^\bullet \\ u_k^\bullet \end{bmatrix}dy - \Delta\int_{y_j}^{y_k} \begin{bmatrix} \psi_j \\ \psi_k \end{bmatrix}dy = 0 \tag{15}$$

where the prime and dot denote the differentiation with respect to y and t, respectively. Simplified Eq. (15) yields:

$$\frac{1}{l^{(e)}}\begin{bmatrix} 1 & -1 \\ -1 & 1 \end{bmatrix}\begin{bmatrix} u_j \\ u_k \end{bmatrix} - \frac{1}{2}\begin{bmatrix} -1 & 1 \\ -1 & 1 \end{bmatrix}\begin{bmatrix} u_j \\ u_k \end{bmatrix} + \frac{Hl^{(e)}}{6}\begin{bmatrix} 2 & 1 \\ 1 & 2 \end{bmatrix}\begin{bmatrix} u_j \\ u_k \end{bmatrix} + \frac{l^{(e)}}{6}\begin{bmatrix} 2 & 1 \\ 1 & 2 \end{bmatrix}\begin{bmatrix} u_j^\bullet \\ u_k^\bullet \end{bmatrix} = \Delta\frac{l^{(e)}}{2}\begin{bmatrix} 1 \\ 1 \end{bmatrix}$$

where $l^{(e)} = y_k - y_j$ is the length of the element (e). In order to get the difference equation at the node i, we write the element equations for two consecutive elements $y_{i-1} \leq y \leq y_i$ and $y_i \leq y \leq y_{i+1}$, assembling the resulting two element equations, one gets:

$$\frac{1}{l^{(e)}}\begin{bmatrix} 1 & -1 & 0 \\ -1 & 2 & -1 \\ 0 & -1 & 1 \end{bmatrix}\begin{bmatrix} u_{i-1} \\ u_i \\ u_{i+1} \end{bmatrix} - \frac{1}{2}\begin{bmatrix} -1 & 1 & 0 \\ -1 & 0 & 1 \\ 0 & 1 & 1 \end{bmatrix}\begin{bmatrix} u_{i-1} \\ u_i \\ u_{i+1} \end{bmatrix} + \frac{Hl^{(e)}}{6}\begin{bmatrix} 2 & 1 & 0 \\ 1 & 4 & 1 \\ 0 & 1 & 2 \end{bmatrix}\begin{bmatrix} u_{i-1} \\ u_i \\ u_{i+1} \end{bmatrix}$$

$$+\frac{l^{(e)}}{6}\begin{bmatrix} 2 & 1 & 0 \\ 1 & 4 & 1 \\ 0 & 1 & 2 \end{bmatrix}\begin{bmatrix} u_{i-1}^\bullet \\ u_i^\bullet \\ u_{i+1}^\bullet \end{bmatrix} = \Delta\frac{l^{(e)}}{2}\begin{bmatrix} 1 \\ 2 \\ 1 \end{bmatrix} \tag{16}$$

Inserting row corresponding to the node i to zero in Eq.(16), the following difference schemes with $l^{(e)} = h$ are obtained:

$$\frac{6}{h^2}(-u_{i-1} + 2u_i - u_{i+1}) - \frac{3}{h}(-u_{i-1} + u_{i+1}) + H(u_{i-1} + 4u_i + u_{i+1}) +$$

$$(u_{i-1}^\bullet + 4u_i^\bullet + u_{i+1}^\bullet) = 6\Delta \tag{17}$$

Applying the trapezoidal rule to Eq. (17) we obtain the following system of equations in the Crank-Nicholson method:

$$A_1 u_{i-1}^{j+1} + A_2 u_i^{j+1} + A_3 u_{i+1}^{j+1} = A_4 u_{i-1}^j + A_5 u_i^j + A_6 u_{i+1}^j + \Omega_{1i}^j \tag{18}$$

Applying the similar procedure to Eqs. (11) and (12) we obtain:

$$B_1 \theta_{i-1}^{j+1} + B_2 \theta_i^{j+1} + B_3 \theta_{i+1}^{j+1} = B_4 \theta_{i-1}^j + B_5 \theta_i^j + B_6 \theta_{i+1}^j + \Omega_{2i}^j \tag{19}$$

$$C_1 \phi_{i-1}^{j+1} + C_2 \phi_i^{j+1} + C_3 \phi_{i+1}^{j+1} = C_4 \phi_{i-1}^j + C_5 \phi_i^j + C_6 \phi_{i+1}^j + \Omega_{3i}^j \tag{20}$$

where

$$A_1 = 1 - 3r + \frac{3}{2} rh + \frac{1}{2} rHh^2; A_2 = 4 + 6r + 2rHh^2; A_3 = 1 - 3r - \frac{3}{2} rh + \frac{1}{2} rHh^2$$

$$A_4 = 1 + 3r - \frac{3}{2} rh - \frac{1}{2} rHh^2; A_5 = 4 - 6r - 2rHh^2; A_6 = 1 + 3r + \frac{3}{2} rh - \frac{1}{2} rHh^2$$

$$B_1 = F^* - 3r + \frac{3}{2} rF^* h; B_2 = 4F^* + 6r; B_3 = F^* - 3r - \frac{3}{2} rF^* h$$

$$B_4 = F^* + 3r - \frac{3}{2} rF^* h; B_5 = 4F^* - 6r; B_6 = F^* + 3r + \frac{3}{2} rF^* h$$

$$C_1 = S_c - 3r + \frac{3}{2} rS_c h; C_2 = 4S_c + 6r; C_3 = S_c - 3r - \frac{3}{2} rS_c h$$

$$C_4 = S_c + 3r - \frac{3}{2} rS_c h; C_5 = 4S_c - 6r; C_6 = S_c + 3r + \frac{3}{2} rS_c h$$

$$\Omega_{1i}^j = 6kG_r(\theta_i^j + N\phi_i^j); \Omega_{2i}^j = 6rF^* D_u(\phi_{i-1}^j - 2\phi_i^j + \phi_{i+1}^j); \Omega_{3i}^j = 6rS_c S_r(\theta_{i-1}^j - 2\theta_i^j + \theta_{i+1}^j)$$

Here, $r = {k}/{h^2}$ and h, k are mesh sizes along $y-$ direction and time $t-$ direction, respectively.

Index i refers to the space and j refers to the time. In Eqs. (18), (19) and (20) taking $i = 1(1)n$ and using boundary conditions (13), the following tri-diagonal systems of equations are obtained:

$$Au = A' \tag{21}$$

$$B\theta = B' \tag{22}$$

$$C\phi = C' \tag{23}$$

where A, B and C are tri-diagonal matrices of order $- n$ and whose elements are given by:

$$A_{i,i} = A_2; B_{i,i} = B_2; C_{i,i} = C_2 \rightarrow \quad \text{at} \quad i = 1(1)n$$

$$A_{i-1,i} = A_1; B_{i-1,i} = B_1; C_{i-1,i} = C_1 \rightarrow \quad \text{at} \quad i = 2(1)n$$

$$A_{i,i+1} = A_3; B_{i,i+1} = B_3; C_{i,i+1} = C_3 \rightarrow \quad \text{at} \quad i = 2(1)n$$

Here, u, θ, ϕ and A', B', C' are column matrices having n-components, namely $u_i^{j+1}, \theta_i^{j+1}, \phi_i^{j+1}$ and $u_i^{j}, \theta_i^{j}, \phi_i^{j}$ respectively. The Gauss-Seidel iteration scheme is employed to solve the above matrix system of equations (21) - (23). Numerical solutions for the velocity, temperature and concentration profiles are obtained by using $C-$ program. The boundary condition $y \to \infty$ is approximated by $y_{max} = 5$, which is sufficiently large for the velocity to approach convergence criterion. The computations are carried out until the steady state is reached. The steady state solution is assumed to have been reached when $\left| u_i^{j+1} - u_i^{j} \right| < 10^{-5}$, $\left| \theta_i^{j+1} - \theta_i^{j} \right| < 10^{-5}$ and $\left| \phi_i^{j+1} - \phi_i^{j} \right| < 10^{-5}$ at all nodal points. To judge the convergence of the Galerkin finite element method, computations are carried out by making small changes in the values of h and k by running the same program, no significant change was observed in the values of u, θ and ϕ. Hence, we conclude that the Galerkin FEM is convergent and stable.

The skin-friction coefficient (τ) at the plate is $\tau = \left(\dfrac{\partial u}{\partial y} \right)_{y=0}$

The heat transfer coefficient (Nu) at the plate is $Nu = -\left(\dfrac{\partial \theta}{\partial y} \right)_{y=0}$

The mass transfer coefficient (Sh) at the plate is $Sh = -\left(\dfrac{\partial \phi}{\partial y} \right)_{y=0}$

4. Results and discussion

To gain a perspective of the physics of the flow regime, we have computed numerical results to study the effects of the physical parameters such as Grashof number G_r, buoyancy ratio N, magnetic parameter M, permeability parameter K, Prandtl number P_r, radiation parameter R, Dufour number D_u, Schmidt number S_c, Soret number S_r, and time parameter t on the velocity u, temperature θ and concentration ϕ as well as the skin-friction, rate of heat and mass transfer. The obtained numerical results have been presented graphically in figures and tables. During the numerical computations, the values of the Prandtl number are chosen $P_r = 0.71, 1.00$ and 7.00, which corresponds to air, electrolytic solution and water at $20^0 C$ and one atmosphere pressure and values of the Schmidt number are taken $S_c = 0.22, 0.60$ and 0.78 which corresponds to hydrogen, water-vapour and ammonia, respectively. The other physical parameters are considered as: $K = 1.0, R = 0.5, D_u = 0.03, S_r = 0.5$ at time $t = 0.5$. These values are kept as common in the entire investigation except variations in respective figures and tables. Further, our results are compared with the results of Bhagwath et al. (2010) and found to be in good agreement in the absence of radiation and Dufour effects.

4.1 Temperature profiles

The effects of the Prandtl number P_r on the temperature profiles are illustrated in Fig.2. It is seen that an increase in the Prandtl number leads to decreases in the temperature profiles. Physically, the increase of P_r decreases the thermal conductivity of the fluid and increases the fluid viscosity, which results in a decrease in the thermal boundary layer thickness. The effects of radiation parameter R on the temperature profiles are presented in Fig.3. It can be seen that the temperature θ increases as the radiation parameter R increases. This is due to the fact that the large R values correspond to an increased dominance of conduction over radiation thereby increasing the thickness of the thermal boundary layer. The influence of the Dufour number D_u on the temperature profiles are shown in Fig.4. It can be noticed that the temperature θ increases in the boundary layer with increasing values of Dufour number. From Fig.5 we can observe= the variation of the temperature profiles for different values of dimensionless time t. The fluid temperature θ is enhanced in the boundary layer with an increase in the boundary layer thickness as the time t increases.
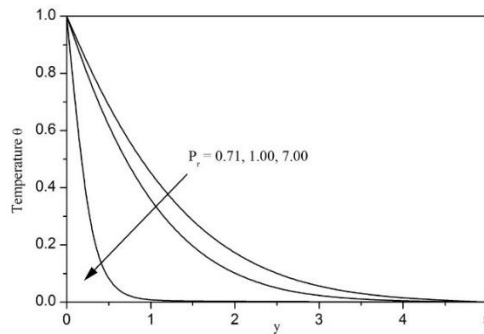
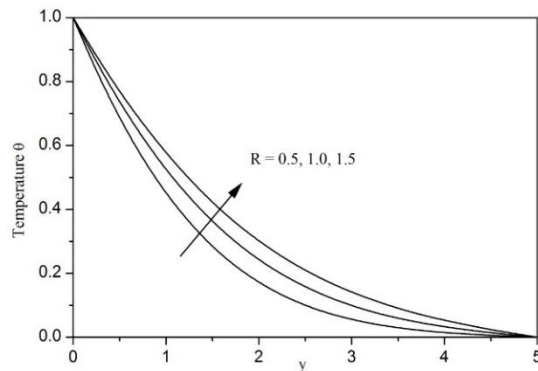**Fig. 2.** Temperature profiles for different values of the Prandtl number P_r

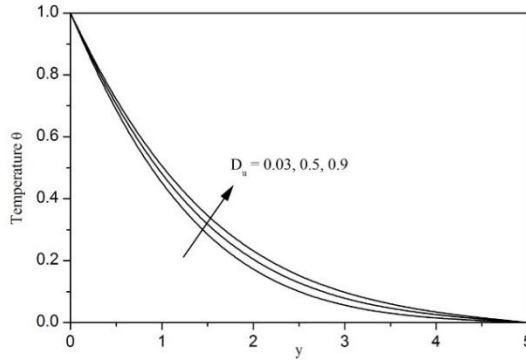**Fig. 3.** Temperature profiles for different values of the radiation parameter R

Fig. 4. Temperature profiles for different values of the Dufour number D_u
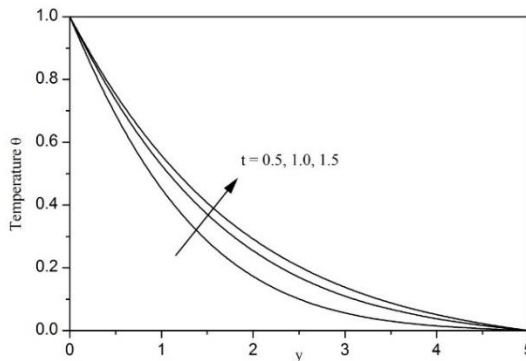

Fig. 5. Temperature profiles for different values of the time parameter t

4.2 Concentration profiles

The effect of the Schmidt number S_c on the concentration profiles are presented in Fig. 6. It can be seen that with increasing value of the Schmidt number concentration decreases. Physically, increase in the Schmidt number leads to a decrease of molecular diffusivity which results in a decrease of concentration boundary layer. Hence, the concentrations of the species are higher for small values of S_c and lower for large values of S_c. The variation of the concentration profiles with Soret number S_r is presented in Fig. 7. It is noticed that there is a marked effect of increasing values of Soret number S_r on the concentration distribution in the boundary layer. It is seen that the concentration profiles increase with increasing values of S_r. These results are in a very good agreement with the results of Vempati and Narayana (2010) in the absence of oscillatory suction velocity. The effects of the time parameter t on the concentration ϕ are presented in Fig.8. It is seen that the concentration profiles increase with increasing time parameter t. Further, this figure verifies the boundary conditions of concentration given in Eq. (13) Initially, concentration takes the value 1 and later for large value of $y(y > 0)$ it tends to zero with increase of time t.
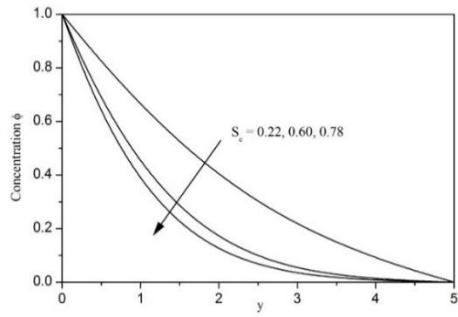
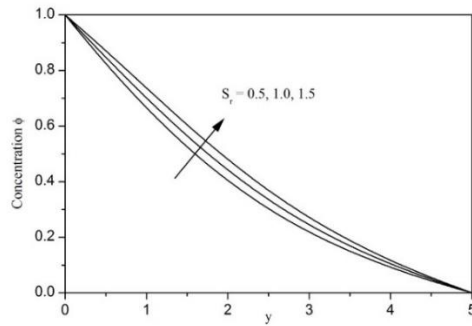**Fig. 6.** Concentration profiles for different values of the Schmidt number S_c

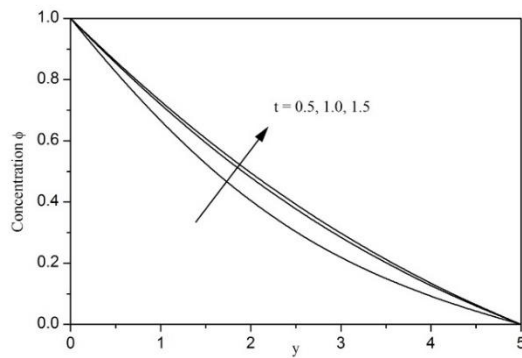**Fig. 7.** Concentration profiles for different values of the Soret number S_r

Fig. 8. Concentration profiles for different values of the time parameter t

4.3 Velocity profiles

The effect of the magnetic parameter M on the velocity profiles can be seen from Fig. 9. The velocity curves show that the rate of transport is remarkably reduced with increasing values of the magnetic parameter indicating that the magnetic field tends to retard the motion of the fluid. Magnetic field may control the flow characteristics. The variation of the velocity profiles with dimensionless permeability parameter K is presented in Fig. 10. It can be noticed that the fluid velocity increases with increasing values of permeability parameter. Physically, this result can be achieved when the holes of the porous medium are very large so that the resistance of the medium may be neglected. It is seen from Fig. 11 that the fluid velocity increases with increasing values of the buoyancy ratio N in the boundary layer. The effects of the Dufour number D_u on the velocity profiles are illustrated in Fig. 12. It can be seen that an increase in the Dufour number from 0.03 to 0.5 and then $0.9,$ increases the fluid velocity in the boundary layer.
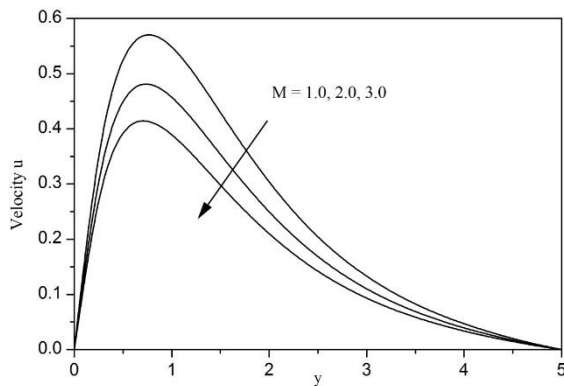

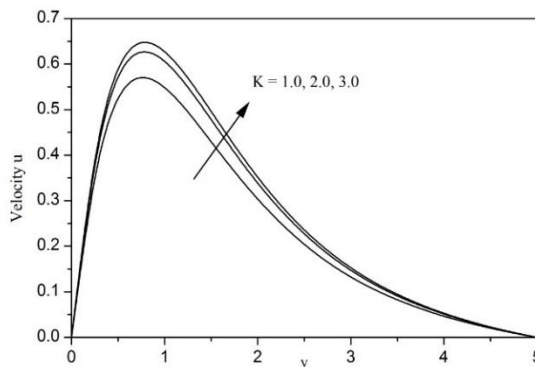**Fig. 9.** Velocity profiles for different values of the magnetic parameter M

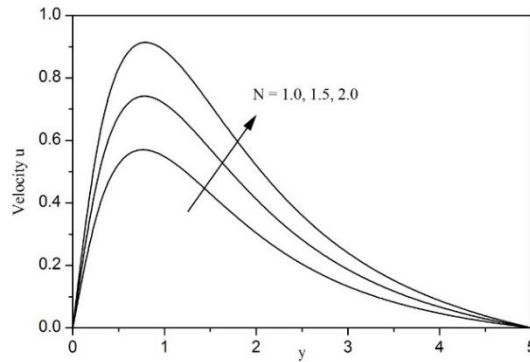**Fig. 10.** Velocity profiles for different values of the permeability parameter K

Fig. 11. Velocity profiles for different values of the buoyancy ratio parameter N
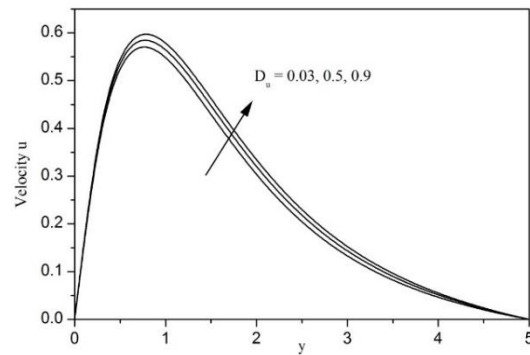

Fig. 12. Velocity profiles for different values of the Dufour number D_u

The effects of Soret number S_r on the velocity profiles are shown in Fig.13. It can be seen that the fluid velocity increases with increasing values of Soret number. It can be seen from Fig. 14 that the fluid velocity increases with increasing radiation parameter R. This is due to the fact that the large values of R correspond to an increased dominance of conduction over radiation thereby increasing buoyancy force and thickness of the momentum boundary layer. The effects of Prandtl number P_r on the velocity profiles can be seen in Fig.15. It is noticed that an increase in the Prandtl number decreases the fluid velocity. This result occurs due to the fact that the fluid with large P_r has high viscosity and small thermal conductivity, which makes the fluid thick and causes a decrease in the fluid velocity. The influence of the Schmidt number S_c on the velocity profiles are shown in Fig. 16. It can be seen that the velocity of the fluid decreases with increasing values of S_c. This is due to the fact that increase of S_c leads to decrease of molecular diffusivity, which results in a decrease in the concentration and velocity boundary layer thickness.
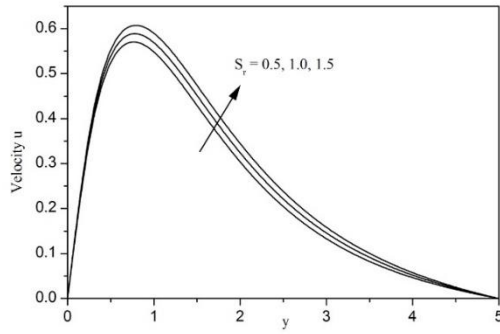
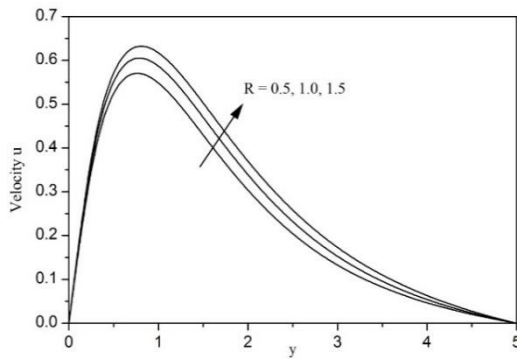**Fig. 13.** Velocity profiles for different values of the Soret number S_r

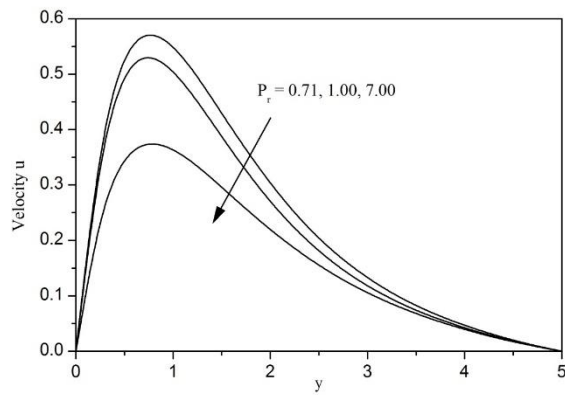**Fig. 14.** Velocity profiles for different values of the radiation parameter R

Fig. 15. Velocity profiles for different values of the Prandtl number P_r
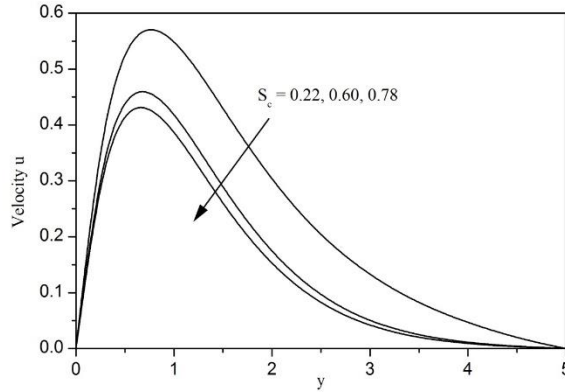
Fig. 16. Velocity profiles for different values of the Schmidt number S_c

The variation of the velocity profiles with Grashof number G_r is presented in Fig. 17. It is seen that the fluid velocity increases with increasing Grashof number. This is due to the fact that buoyancy force enhances the fluid velocity and increases the boundary layer thickness with increase in the value of Grashof number. The variation of the velocity profiles for different values of dimensionless time t is shown in Fig. 18. It is noticed that the fluid velocity increases with the progression of time t. Moreover, the velocity in this figure takes the values of time t at the plate $(y = 0)$ and tends to zero for large values of y, which is a clear verification of the boundary conditions on the velocity u is given in Eq. (13)
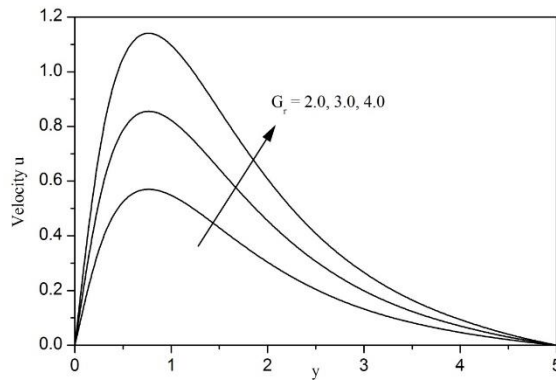

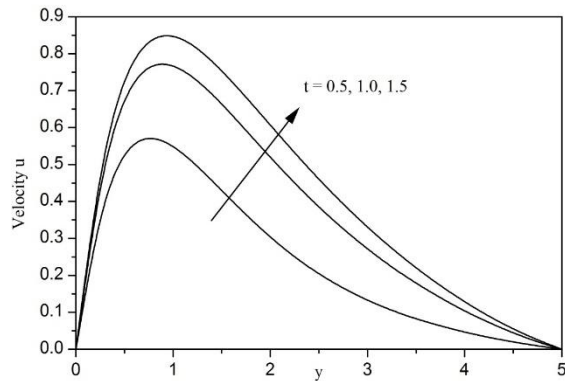**Fig. 17.** Velocity profiles for different values of the Grashof number G_r

Fig. 18. Velocity profiles for different values of the time parameter t

4.4 Skin-friction, Nusselt and Sherwood numbers

Numerical data for the skin-friction coefficient (τ), Nusselt number (Nu) and Sherwood number (Sh) for variation in the material parameters are presented in the Tables 1-3. Table 1 shows that the skin-friction increases with increasing values of the radiation parameter, Dufour number, buoyancy ratio, permeability parameter, Soret number, Grashof number and time parameter whereas it decreases with increasing values of the Prandtl number, Schmidt number and magnetic parameter. It is noticed from Table 2 that the values of the Nusselt number increases with increasing Prandtl number and decreases with increasing radiation parameter, Dufour number and time parameter. It is seen from Table 3 that an increase in Schmidt number leads to increase in the Sherwood number and decreases with increase in Soret number and time parameter.

P_r	S_c	R	D_u	S_r	N	M	K	G_r	t	τ
0.71	0.22	0.5	0.03	0.5	1.0	1.0	1.0	2.0	0.5	0.771748
7.00	0.22	0.5	0.03	0.5	1.0	1.0	1.0	2.0	0.5	0.513562
0.71	0.60	0.5	0.03	0.5	1.0	1.0	1.0	2.0	0.5	0.610300
0.71	0.22	1.0	0.03	0.5	1.0	1.0	1.0	2.0	0.5	0.803226
0.71	0.22	0.5	0.50	0.5	1.0	1.0	1.0	2.0	0.5	0.784416
0.71	0.22	0.5	0.03	1.0	1.0	1.0	1.0	2.0	0.5	0.788234
0.71	0.22	0.5	0.03	0.5	1.5	1.0	1.0	2.0	0.5	0.990294
0.71	0.22	0.5	0.03	0.5	1.0	2.0	1.0	2.0	0.5	0.675460
0.71	0.22	0.5	0.03	0.5	1.0	1.0	2.0	2.0	0.5	0.831082
0.71	0.22	0.5	0.03	0.5	1.0	1.0	1.0	3.0	0.5	1.157622
0.71	0.22	0.5	0.03	0.5	1.0	1.0	1.0	2.0	1.0	0.946308

Table 1. Numerical data for the skin-friction coefficient (τ)

P_r	R	D_u	t	Nu
0.71	0.5	0.03	0.5	0.337380
7.00	0.5	0.03	0.5	1.510984
0.71	1.0	0.03	0.5	0.275234
0.71	0.5	0.50	0.5	0.316636
0.71	0.5	0.03	1.0	0.285110

Table 2. Numerical data for the Nusselt number (Nu)

S_c	S_r	t	Sh
0.22	0.5	0.5	0.179692
0.60	0.5	0.5	0.334116
0.22	1.0	0.5	0.153074
0.22	0.5	0.5	0.148350

Table 3. Numerical data for the Sherwood number (Sh)

5. Conclusions

In this paper, the Dufour and Soret effects on unsteady MHD free convection heat and mass transfer flow past an infinite vertical porous plate in the presence of radiation are provided. The dimensionless governing equations of the flow have been solved numerically by applying Galerkin FEM. It is shown that the flow characteristics are influenced by the material parameters involved in the problem. It has been found that the fluid velocity and temperature decrease when the Prandtl number increases whereas an increase in the radiation parameter enhances the fluid velocity and temperature in the boundary layer. The fluid velocity increases with increasing Dufour and Soret numbers. An increase in the Schmidt number leads to a decrease in the fluid velocity and concentration. Influence of the magnetic parameter decelerates the fluid velocity. Further, the velocity, temperature and concentration increase with increasing time parameter. The present study of the physics of the fluid flow could be useful in the scientific and engineering applications.

References

Ahmed N, Sarmah H K (2009). Thermal radiation effects on a transient MHD flow with mass transfer past an impulsively fixed infinite vertical plate, *Int. J. Appl. Math and Mech.*, 5(5), 87 – 98.

Alam M S, Rahman M M (2005). Dufour and Soret effects on MHD free convective heat and mass transfer flow past a vertical flat plate embedded in a porous medium, *J. Naval Architecture and Marine Engineering.*, 2(1), 55 - 65.

Alam M S, Rahman M M, Samad M A (2006). Dufour and Soret effects on unsteady MHD free convection and mass transfer flow past a vertical porous plate in a porous medium, *Nonlinear Analysis, Modeling and Control.,* 11(3), 217 - 226.

Alam M S, Rahman M M, Maleque A, Ferdows M (2006). Dufour and Soret effects on steady MHD combined free-force convective and mass transfer flow past a semi-infinite vertical plate, *Thammasat Int. J. Science and Technology.,* 11(2), 1-12.

Anghel M, Takhar H S, Pop I (2000). Dufour and Soret effects on free convection boundary layer over a vertical surface embedded in a porous medium, *Studia Universitatis Babes-Balyai, Mathematica*, Vol.XLV (4), 11-21.

Ananad Rao J, Prabhakar Reddy B (2010). Finite element analysis of heat and mass transfer of an unsteady MHD natural convection flow of a rotating fluid past a vertical porous plate in the presence of radiative heat transfer, *J. Energy, Heat and Mass Transfer.,* 32, 223 – 241.

Bhagwat S, Kumar P, Jha R (2010). Effects of thermal diffusion on MHD free convective flow past a vertical porous plate, *Int. J. Stability and Fluid Mech.,* 1 (1), 43 – 54.

Chamkha A J, Takhar H S, Beg O A (2004). Radiative free convective non-Newtonian fluid flow past a wedge embedded in a porous media., *Int. J. Fluid Mech. Research*, 31, 101- 115.

Dursunkaya Z, Worek W M (1992). Diffusion-thermo and thermal-diffusion effects on transient and steady natural convection from vertical surface, *Int. J. Heat and Mass Transfer.,* 35(8), 2060 - 2065.

Eckert F R C, Drake R M (1972). *Analysis of heat and mass transfer,* McGraw-Hill, New York.

Mansour M A, El-Anssary N F, Aly A M (2006). Effects of chemical reaction and thermal stratification on MHD free convective heat and mass transfer over a vertical stretching surface embedded in a porous media considering Soret and Dufour numbers, *J. Chemical Engineering*., 145(2) 340 - 345.

Mahmoud M A A (2009). Thermal radiation effects on unsteady MHD free convection flow past a vertical plate with temperature dependent viscosity, *Canadian J. Chem. Engineering.,* 87, 47 - 52.

Muthucumaraswamy R, Janakiraman (2006). MHD and radiation effects on moving isothermal vertical plate with variable mass diffusion, Theoret. *Appl. Mech.,* 33, 17 – 29.

Mukhopadhyay S (2009). The effects of thermal radiation on unsteady mixed convection flow and heat transfer over a porous stretching surface in porous medium, *Int. J. Heat and Mass Transfer.,* 52, 3261 – 3265.

Muthucumaraswamy R, Sivakaumar P (2016). MHD flow past a parabolic flow past an infinite isothermal vertical plate in the presence of thermal radiation and chemical reaction, *Int. J. Appl. Mech. and Engg.,* 21 (1), 95 – 105.

Postelnicu A (2004). Influence of a magnetic field on heat and mass transfer by natural convection from vertical surface in porous media by considering Soret and Dufour effects, *Int. J. Heat and Mass Transfer.,* 47(.6-7), 1467-1472.

Prabhakar Reddy B (2014). Effects of thermal diffusion and viscous dissipation on unsteady NHD free convection flow past a vertical porous plate under oscillatory suction velocity, *Int. J. Appl. Mech. and Engg*., 19(2), 303 - 320.

Reddy J N (2005). *An introduction to the finite element method*, 3rd Ed., Mac-Graw Hill, New York.

Seth G S, Ansari M D S, Nandkeolyer R (2010). MHD natural convection flow past an impulsively moving vertical plate with ramped wall temperature in the presence of thermal diffusion and heat absorption, Int. *J. Appl. Mech and Engg.,* 15, 199 - 215.

Shanker R T, Gnaneshwar R M (2007). Radiation effects on MHD flow past an impulsively started infinite vertical plate through a porous medium with variable temperature and mass diffusion, *J. Pure and Appl. Phys.,* 19 (3), 191 – 200.

Shanaker B, Prabhakar Reddy B, Ananad Rao J (2010). Radiation and mass transfer effects on unsteady MHD free convective fluid flow embedded in a porous medium with heat generation/absorption, *Indian J. Pure and Appl. Phys.,* 48, 157-165.

Vempati S R, Laxmi Narayana Gari A B (2010). Soret and Dufour effects on unsteady MHD flow past an infinite vertical porous plate with thermal radiation, *Appl. Math. Mech-* Engl. Ed., 31(12), 1481-1496.

Venkateswarlu M, Ramana Reddy G V, Laxmi D V (2014). Thermal diffusion and radiation effects on unsteady MHD free convection heat and mass transfer flow past a linearly accelerated vertical porous plate with variable temperature and mass diffusion, *The Korea Society for Industrial and Applied mathematics*., 183, 257- 268.